PRODUCTION AND CORRELATIONS OF STRANGE MESONS AND BARYONS AT RHIC AND LHC IN HYDROKINETIC MODEL

Yu.M. Sinyukov[a,b,c], V.M. Shapoval[a]

[a]Bogolyubov Institute for Theoretical Physics
Metrolohichna 14b, 03680 Kiev, Ukraine
[b]ExtreMe Matter Institute EMMI
GSI Helmholtzzentrum für Schwerionenforschung
64291 Darmstadt, Germany
[c]Tomsk State University, Department of Physics
Lenin ave. 36, Tomsk, Russia

(Received June 6, 2016)

Dedicated to Andrzej Bialas in honour of his 80th birthday

The recent results on the theoretical analysis of particle production and correlation in relativistic heavy-ion collisions at the LHC and RHIC within the hydrokinetic model (HKM) and its extended version — integrated hydrokinetic model (iHKM) are addressed. The study of strange K meson spectrum and femtoscopy scales is discussed along with the pion ones for the case of LHC Pb+Pb collisions at $\sqrt{s_{NN}} = 2.76$ TeV. The $m_{\rm T}$-dependence of spectra and longitudinal femtoscopy scales at the LHC, obtained in HKM simulations, is compared with the results given by simple analytical formulas including the effective temperature on the hypersurface of maximal particle emission, emission proper time, and transverse flow intensity. The influence of $K^*(892)$ resonance decays and hadron re-scatterings at the afterburner stage of the collision on the interferometry radii is analyzed. The related problem of $K^*(892)$ effective identification and reliable yield measurement in view of hadron re-scatterings is also investigated for RHIC and LHC energy cases. The application of the FSI formalism with account for residual correlation effect to modeling of the $p\Lambda$ and $p\Xi$ correlation functions using the source functions calculated in HKM is also considered.

DOI:10.5506/APhysPolB.47.1883

1. Introduction

The study of spatiotemporal extents of the emission sources for different particle species, produced in relativistic heavy-ion collisions, serves as a good instrument for the study of the properties of hot and dense matter created in these processes, since the structure of particle emission is essentially defined by the collision dynamics [1–4]. The most common direct method for such an analysis is the correlation femtoscopy or intensity interferometry [5], which allows one to measure the interferometry radii, associated with the homogeneity lengths of a particle emission region. They are usually extracted from a Gaussian fit to the two-particle momentum correlation function. Determining the dependence of the femtoscopy scales on pair transverse average momentum $k_{\rm T} = |\boldsymbol{p}_{\rm T1} + \boldsymbol{p}_{\rm T2}|/2$ or transverse mass $m_{\rm T}$ ($m_{\rm T}^2 = m^2 + (|\boldsymbol{p}_{\rm T1} + \boldsymbol{p}_{\rm T2}|/2)^2 = m^2 + k_{\rm T}^2$) for different particle species allows to test the applicability of different matter evolution scenarios and particle emission pictures in the collision process. For instance, if one supposes the hydrodynamic approximation with negligible transverse flow to be justified for $A + A$ collision, then the longitudinal radii $R_{\rm L}(m_{\rm T})$ should have similar $m_{\rm T}^{-1/2}$ behavior for pions and kaons, even up to complete $m_{\rm T}$-scaling in the common freeze-out case [2, 3]. However, in reality, the particle emission picture is much more complicated and the results are a product of interplay of a number of various factors, and it requires a thorough analysis to be performed in a very detailed $A + A$ collision model.

The hydrokinetic model (HKM) [6], which simulates the evolution process of the system formed in relativistic heavy-ion collisions, was designed to describe and predict different bulk observables measured in experiments at RHIC and LHC. In particular, a good description was obtained in HKM for pion, kaon, proton and all charged particle spectra at different centralities together with the corresponding elliptic flows [6]. A prediction as for reduction of the $R_{\rm out}/R_{\rm side}$ ratio at the LHC as compared to the RHIC was made in HKM [7] and then experimentally confirmed. The pion and kaon femtoscopic scales at RHIC [6, 8] and LHC [6, 9] were also calculated in the model. Moreover, not only the interferometry radii, but also the non-Gaussian source functions for pions and kaons were successfully described for the top RHIC energy and predicted for the LHC one [10]. In addition to the results related to heavy-ion collision, a good description of pion interferometry radii in the LHC $p + p$ collisions at $\sqrt{s} = 7$ TeV was reached in hydrokinetic model with the quantum uncertainty principle corrections applied to a quasi-classical event generator results [11].

As for the $m_{\rm T}$-scaling between pion and kaon femtoscopy radii at the LHC, HKM predicts [9] that it is violated, and the $k_{\rm T}$ scaling (for $k_{\rm T} > k_0 \approx 0.4$ GeV/c) takes place instead. The reasons for such a behavior are

analyzed within HKM in [12] and the results of that study are discussed in the current paper below. It appears that the breaking of m_{T}-scaling is caused by the interplay of the following factors: strong transverse collective flows, non-Gaussian shape of the correlation function, particle re-scatterings and resonance decays at the afterburner stage of the system's evolution, where produced particles continue to re-scatter and annihilate, gradually escaping from the fireball to finally travel towards the detectors without interaction.

The intensity of particle collisions at the afterburner stage can be probed by analyzing the effectiveness of strange $K(892)^*$ resonances registration by their decays into $K\pi$ pairs. The point is that the interactions between daughter hadrons do not allow to identify all the produced K^*s, so the resulting fraction of restored resonances strongly depends on the hadron interaction intensity at 3–5 fm/c after the afterburner stage beginning. In addition, the experimental particle number ratios, regarded as a source of information about the collision dynamics and the properties of matter at the chemical freeze-out (at the temperature $T \approx 160$ MeV), also diverge from their true values. In this paper, we consider how the hadronic re-scatterings at the afterburner stage affect the observability of strange $K(892)^*$ resonance utilizing the integrated hydrokinetic model (iHKM) for the case of Pb+Pb collisions at the LHC. We consider different centrality classes at the collision energy $\sqrt{s_{NN}} = 2.76$ TeV. The calculation results for the LHC case are then compared with experimental data from RHIC presented by the STAR Collaboration.

At last, we deal with the problem of the final state interaction (FSI) analysis of baryon–(anti)baryon correlations. Namely, taking the results obtained earlier within the Lednicky–Lyuboshitz analytical model for the $p\Lambda$ case as a starting point, we present theoretical predictions as for the $p\Xi$ correlation functions (CF), obtained within the so-called Koonin–Pratt (KP) formalism. In this approach, the pair CF is expressed through the squared modulus of the pair relative wave-function averaged over the Gaussian time-integrated pair separation distribution (the source function). The latter is defined by the source radius, extracted from the fit to the source function calculated in iHKM. The effect of residual correlations is also taken into account using an effective analytical approximation introduced as an additional term into the model expression for the correlation function.

2. π and K meson spectra and femtoscopy scales

2.1. Analytical formula for femtoscopy scales

The system's evolution simulation in hydrokinetic model consists of two stages — the hydrodynamic expansion of the (locally) thermally and chemically equilibrated matter and gradual system decoupling, which starts when

the equilibrium gets lost. For the description of the first stage, the ideal hydrodynamics approximation is utilized and the second one is described within the hydrokinetic approach, based on the integral Boltzmann equations. Then, on some spacelike hypersurface, one performs switching to UrQMD hadronic cascade [13]. For the calculations presented here, the simplified HKM variant is utilized [14], where a sudden switch is performed from collective matter evolution to a particle cascade at the hadronization hypersurface, chosen to be the isotherm $T = 165$ MeV. As a result of the model, one gets a set of produced particle momenta and coordinates that serve for building necessary observables.

The initial conditions for the hydro evolution in HKM are set by specifying the initial transverse energy density profile $\epsilon_0(\boldsymbol{r}_{\mathrm{T}})$ and the initial transverse flow $y_0(\boldsymbol{r}_{\mathrm{T}})$ at the initial proper time τ_0. For the case of $A + A$ collisions, we take $\tau_0 = 0.1$ fm/c, and $\epsilon_0(\boldsymbol{r}_{\mathrm{T}})$ is generated in GLISSANDO MC Glauber code [15]. The normalization constant ϵ_0, being the maximal initial energy density, is fixed from the mean charged particle multiplicity in the considered experiment.

In order to analyze the role of different factors in defining the particle emission picture in HKM and find the way of determination of the approximate particle maximal emission time in the experiment, we consider here the logic of the spectra formation and some analytical estimates for the spectra and femtoscopy scales. In the hydrodynamic approach based on Boltzmann equations [16, 17], it can be shown that, although the freeze-out in general case has a finite time width, the momentum spectra are still well-described within the Cooper–Frye prescription (CFp) [18]. In such a case, the freeze-out duration is defined by the inverse of the particle collision rate at the maximal emission points for particles with momentum p, $(t_\sigma(\boldsymbol{r}, p), \boldsymbol{r})$. In most cases, the hypersurface consisting of all such points does not completely enclose the originally dense matter. Since for each concrete p the related hypersurface piece σ_p is always spacelike, the utilization of such generalized Cooper–Frye prescription allows to avoid automatically the general problem of standard CFp, namely the negative contributions to the particle spectrum from non-spacelike parts of the common freeze-out hypersurface.

Following the results of [17, 19, 20], let us regard the hypersurface $\tau = \tau_{\mathrm{m.e.}} = \mathrm{const}$ of constant proper time (limited in transverse dimension $\boldsymbol{r}_{\mathrm{T}}$) as the hypersurface of maximal emission for particles with comparably soft momenta p (for the hard momentum particles with $p_{\mathrm{T}} > 0.8$ GeV/c, such hypersurface is not suitable due to space-time correlation presence [19, 20]). Then, the bosonic Wigner function in most central events will be given by

$$f_{\mathrm{l.eq.}}(x, p) = \frac{1}{(2\pi)^3} \left[\exp(\beta p \cdot u(\tau_{\mathrm{m.e.}}, \boldsymbol{r}_{\mathrm{T}}) - \beta\mu) - 1\right]^{-1} \rho(\boldsymbol{r}_{\mathrm{T}}) \qquad (1)$$

with the Gaussian cutoff factor [19, 20], suppressing the contribution from high-momentum particles, emitted from rapidly moving fluid elements with $\cosh\eta_{\rm T}(r_{\rm T}) \gg 1$,

$$\rho(\boldsymbol{r}_{\rm T}) = \exp[-\alpha(\cosh\eta_{\rm T}(r_{\rm T}) - 1)]\,. \tag{2}$$

Here, $\beta = 1/T$ is the temperature reciprocal at $\tau_{\rm m.e.}$, $x^\mu = (\tau\cosh\eta_{\rm L}, \boldsymbol{r}_{\rm T}, \tau\sinh\eta_{\rm L})$ is the 4-coordinate with longitudinal rapidity $\eta_{\rm L} = \operatorname{arctanh} v_{\rm L} = \frac{1}{2}\ln\frac{t+x_{\rm L}}{t-x_{\rm L}}$, transverse rapidity $\eta_{\rm T} = \operatorname{arctanh} v_{\rm T}(r_{\rm T})$, and $u^\mu(x) = (\cosh\eta_{\rm L}\cosh\eta_{\rm T}, \frac{\boldsymbol{r}_{\rm T}}{r_{\rm T}}\sinh\eta_{\rm T}, \sinh\eta_{\rm L}\cosh\eta_{\rm T})$ — the hydrodynamic velocity.

According to [19, 20] and in the view of improved CFp [17], the parameter $\alpha = R_v^2/R_{\rm T}^2$, where $R_{\rm T}$ is the transverse homogeneity length in $r_{\rm T}$ (near $r_{\rm T} = 0$ for small $k_{\rm T}$) along the hypersurface $\tau = \tau_{\rm m.e.} = \text{const}$, and R_v is the hydrodynamic length, $R_v = (v'(r_{\rm T}))^{-1}$, near the same $r_{\rm T}$. The small α means a very intensive flow, such that the hydrodynamic length R_v appears to be much smaller than the homogeneity length $R_{\rm T}$. The case of very large α corresponds to $R_v = \infty$, *i.e.* absence of the transverse flow.

Within introduced formalism, the boson single particle spectrum and the correlation function will be written as follows:

$$p_0\frac{{\rm d}^3N}{{\rm d}^3p} = \int\limits_{\sigma_{\rm m.e.}(p)} {\rm d}\sigma_\mu\, p^\mu f_{\rm l.eq.}(x,p)\,, \tag{3}$$

$$C(p,q) \approx 1 + \frac{\left|\int_{\sigma_{\rm m.e.}(k)} {\rm d}\sigma_\mu\, k^\mu f_{\rm l.eq.}(x,k)\exp(iqx)\right|^2}{\left(\int_{\sigma_{\rm m.e.}(k)} {\rm d}\sigma_\mu\, k^\mu f_{\rm l.eq.}(x,k)\right)^2}\,, \tag{4}$$

where $q = p_1 - p_2$, $k^\mu = \left(\sqrt{m^2 + \left(\frac{\boldsymbol{p}_1+\boldsymbol{p}_2}{2}\right)^2}, \frac{\boldsymbol{p}_1+\boldsymbol{p}_2}{2}\right)$. Here the smoothness and mass shell approximations are applied, so that $k \approx p = (p_1+p_2)/2$ and the 4-vector q has only three independent components. The latter can be selected along the beam axis, $q_{\rm long} \equiv q_{\rm l}$, along the pair transverse momentum vector $\boldsymbol{k}_{\rm T}$, $q_{\rm out} \equiv q_{\rm o}$, and along *side* direction, $q_{\rm side} \equiv q_{\rm s}$, orthogonal to both *long* and *out* directions.

Applying then the saddle point method (in complex plane) to the calculation of the spectra and correlation function (4) in Boltzmann approximation for longitudinally boost-invariant expansion, one will obtain in LCMS [21]

$$C(k, q_{\rm l}, q_{\rm s} = q_{\rm o} = 0) = 1 + \frac{\exp\left[\frac{2}{\lambda^2}\left(1 - \sqrt{1+\tau^2\lambda^4 q_{\rm l}^2}\right)\right]}{\left[1+\tau^2\lambda^4 q_{\rm l}^2\right]^{3/2}} \overset{k_{\rm T}\to\infty}{\longrightarrow} 1 + \exp\left(-\lambda_{\rm L}^2 q_{\rm l}^2\right)\,, \tag{5}$$

where according to [19, 20], λ is defined as

$$\lambda^2 = \frac{\lambda_{\rm L}^2}{\tau^2} = \frac{T}{m_{\rm T}} \left(1 - \bar{v}_{\rm T}^2\right)^{1/2} . \tag{6}$$

Here, $\lambda_{\rm L} = \tau\sqrt{\frac{T}{m_{\rm T}}(1-\bar{v}_{\rm T}^2)^{1/2}}$ is the longitudinal homogeneity length in presence of the transverse flow, $\bar{v}_{\rm T}$ is the transverse velocity in the saddle point, $\bar{v}_{\rm T} = k_{\rm T}/(m_{\rm T}+\alpha T)$, $T = T_{\rm m.e.}$ is the temperature at the hypersurface of maximal emission, $\tau = \tau_{\rm m.e.}$. The dependece on $q_{\rm o}$ and $q_{\rm s}$ is neglected since the correlation function behavior in *long* direction does not depend on the transverse velocity profile at the hypersurface of maximal emission, depending only on the parameter α. The *out* and *side* projections are, on the contrary, quite sensitive to the details of the velocity profile.

At large $m_{\rm T}/T \gg 1$, when the correlation function shape is Gaussian, the interferometry radii coincide with homogeneity lengths. In the case of pure Bjorken expansion (no transverse flow, $\bar{v}_{\rm T} = 0$), one has $R_{\rm L} = \lambda_{\rm L} = \tau\sqrt{\frac{T}{m_{\rm T}}}$ (first obtained in [2]). In [22], the authors proposed the correction to the radii for small $m_{\rm T}/T \approx 1$, probably applicable for pions at zero transverse flow

$$R_{\rm L}^2 = \lambda_{\rm L}^2 \to \lambda_{\rm L}^2 \frac{K_2\left(\frac{m_{\rm T}}{T}\right)}{K_1\left(\frac{m_{\rm T}}{T}\right)} , \tag{7}$$

where K_n are modified Bessel functions. As one can see from (5), at $m_{\rm T}/T \approx 1$, the correlation function is essentially non-Gaussian, so the radius $R_{\rm L}$ describes only the peak of the correlation function, that corresponds to the Gaussian approximation at small $q_{\rm l}$, $C(q_{\rm l}) = 1 + \exp(-R_{\rm L}^2 q_{\rm l}^2)$[1].

Supposing boost-invariant longitudinal expansion, from (5) at small $q_{\rm l}$ one can obtain for the radii at transverse flow with arbitrary velocity profile

$$R_{\rm L}^2(k_{\rm T}) = \tau^2\lambda^2\left(1 + \tfrac{3}{2}\lambda^2\right) . \tag{8}$$

Comparing this result with (7) for pure Bjorken picture ($\alpha \to \infty$ in our notation), we find that the difference between two results in all actual $k_{\rm T}$ intervals for pion pairs is only 1–3%. However, our expression (8) is justified for the case of collective flows of arbitrary intensity, which is important when describing the LHC collisions.

2.2. Fitting the HKM results

Analyzing the $m_{\rm T}$-dependence of $R_{\rm L}$ in the approximation of 1D hydrodynamics, one finds that $m_{\rm T}$-scaling should take place — such radius

[1] For the detailed analysis of different analytical approximations for the femtoscopy scales, see [21].

behavior was obtained already in [2], namely $R_{\mathrm{L}} \propto \sqrt{T/m_{\mathrm{T}}}$. Application of (7) and (8) in this case (it corresponds to $\alpha = \infty \Rightarrow \bar{v}_{\mathrm{T}} = 0$) also results in scaling, $R_{\mathrm{L}} = R_{\mathrm{L}}(\tau, m_{\mathrm{T}}/T)$.

However, the results of HKM simulations for LHC energies show the absence of m_{T} scaling [9]. To investigate the physical reasons leading to this, we calculated the pion and kaon radii in HKM with UrQMD cascade switched off (but with resonance decays still implemented) and tried to fit the obtained points with (8) at $\alpha = \infty$. As one can see, in Fig. 1 the fits are quite bad (χ^2/n.d.f. = 2562.31 for pions and χ^2/n.d.f. = 585.24 for kaons), and there is no m_{T}-scaling as well as in the case of full HKM simulations.

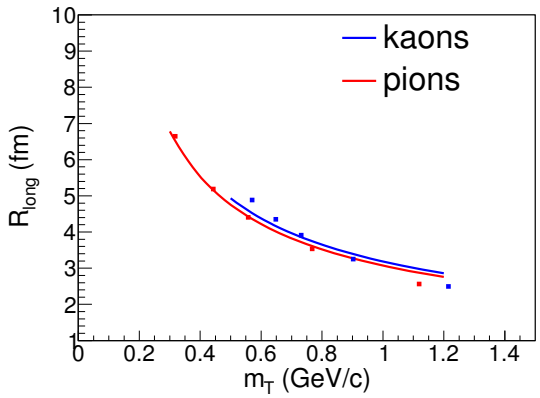

Fig. 1. The m_{T} dependencies of longitudinal femtoscopy radius R_{L} calculated in HKM model without re-scattering stage for $K^{\mathrm{ch}}K^{\mathrm{ch}}$ and $\pi^-\pi^-$ pairs (markers) together with the corresponding fits (lines) according to formula (8) where transverse flow is absent ($\alpha = \infty$). The temperature is $T = 165$ MeV. The results are related to $\sqrt{s_{NN}} = 2.76$ GeV Pb+Pb collisions at the LHC, $c = 0$–5%, $|\eta| < 0.8$, $0.14 < p_{\mathrm{T}} < 1.5$ GeV/c.

The quality of the fits grows dramatically if one sets α in (8) to have a finite value in order to account for non-zero transverse flow (see Fig. 2). Now, R_{L} depends on both m_{T}/T and k_{T}/T variables, so the scaling between analytical curves disappears. Thus, one of the reasons of m_{T}-scaling violation in HKM is the existence of strong transverse flow in simulations related to LHC heavy-ion collision experiments. The satisfactory pion and kaon radii description is obtained with the same temperature parameter value, $T = 165$ MeV, and maximal emission times $\tau_\pi = 7.41$ fm/c for pions and $\tau_K = 7.56$ fm/c for kaons. For both mesons, $\alpha = 2.8$.

Apart from the transverse flow, scaling can be violated because of non-Gaussian form of the corresponding correlation functions and the re-scattering interactions at the afterburner stage of system's evolution. For analyzing

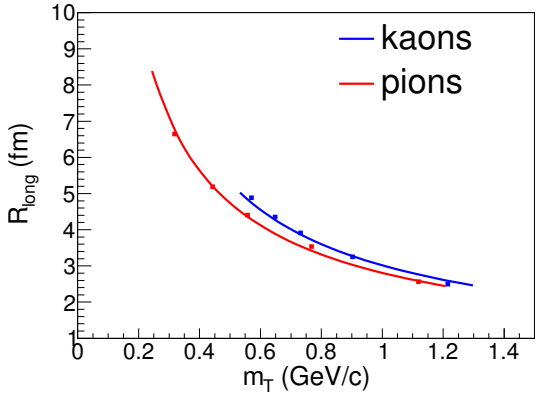

Fig. 2. The same as in Fig. 1 but fits account now for the intensive transverse flow, $\alpha = 2.8$. The time parameters for pions and kaons are $\tau_\pi = 7.41$ fm/c and $\tau_K = 7.56$ fm/c correspondingly, $T_\pi = T_K = 165$ MeV.

the influence of these factors, the results of calculations in full HKM (with UrQMD cascade) should be used. The parameters T and α appearing in the fitting formula for radii can be fixed from the fit to respective particle momentum spectra, *e.g.* from the combined fit to pion and kaon spectra calculated in HKM with account for the transverse flow. Fitting the spectra can be carried out based on the following formula, obtained in the same approximation as (5) [20]

$$p_0 \frac{\mathrm{d}^3 N}{\mathrm{d}^3 p} \propto \exp\left[-\left(m_{\mathrm{T}}/T + \alpha\right)\left(1 - \bar{v}_{\mathrm{T}}^2\right)^{1/2} \right]. \tag{9}$$

Figure 3 shows the result of the combined pion–kaon spectrum fit (9) to HKM points together with the experimental data [23] in p_{T}-range of 0.5–1.0 GeV/c. The temperature parameter was put to be the same for both particle species, and the extracted parameter values are the following: $T = 144 \pm 3$ MeV, $\alpha_\pi = 5.0 \pm 3.5$ and $\alpha_K = 2.2 \pm 0.7$. The obtained values with the respective errrors are substituted then to (8) in order to fit the femtoscopy scales m_{T}-dependence. Since the formulas (7) and (8) are related to the Gaussian radii, describing only the small q region when the correlation function is non-Gaussian, we use the limited fitting range, $q = 0$–0.04 GeV/c, at extraction the interferometry radii from the full HKM. The corresponding radii m_{T} dependence is shown in Fig. 4 together with the analytical fit according to Eq. (8), with T and α constrained based on the combined spectra fit. The pion and kaon times of maximal emission extracted from the fit are $\tau_\pi = 9.44 \pm 0.02$ fm/c and $\tau_K = 12.40 \pm 0.04$ fm/c, respectively, while the rest of parameters take values $T_\pi = 147$ MeV, $T_K = 141$ MeV, $\alpha_\pi = 8.5$ and $\alpha_K = 1.5$.

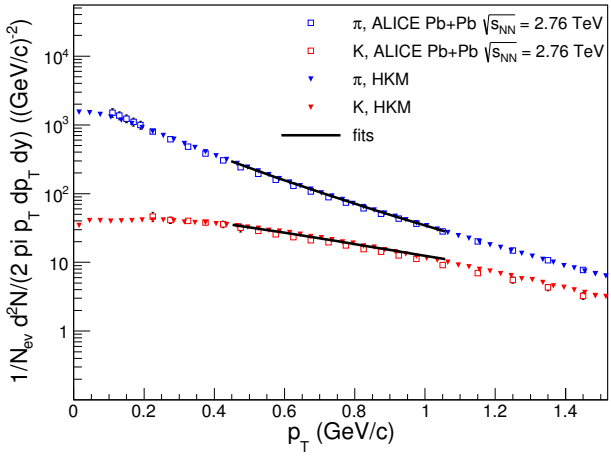

Fig. 3. Pion (upper/blue) and kaon (lower/red) momentum spectra in Pb+Pb collisions at the LHC, $\sqrt{s_{NN}} = 2.76$ GeV. Open squares show experimental values [23], triangles show HKM results, black lines correspond to combined (with the same temperature T) pion and kaon spectra fit according to (9).

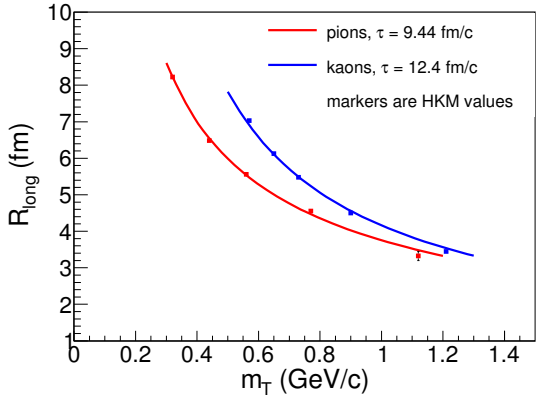

Fig. 4. The same as in Figs. 1 and 2 but radii are calculated in the full HKM model including re-scattering stage. To reduce the effect of the non-Gaussian correlation functions, we take more narrow fitting range for them, q = 0–0.04 GeV/c. The fit parameters T and α correspond to combined pion and kaon spectra fitting. At T_π = 147 MeV, T_K = 141 MeV, α_π = 8.5 and α_K = 1.5, extracted maximal emission times are $\tau_\pi = 9.44 \pm 0.02$ fm/c and $\tau_K = 12.40 \pm 0.04$ fm/c.

Another way of comparison of the pion and kaon emission pictures in HKM is examining the plots based on the respective invariant emission functions $G(x,p) = p^0 \frac{\mathrm{d}^7 N}{\mathrm{d}^4 x \mathrm{d}^3 p}$. In Fig. 5, one can see the reduced emission function

averaged over all momentum angles $g(r_{\rm T},\tau;p_{\rm T}) = \frac{p^0{\rm d}^6N}{{\rm d}r_o{\rm d}r_s{\rm d}\eta{\rm d}\tau{\rm d}p_{\rm T}{\rm d}y}\Big|_{r_s=0}$ for pions and kaons at $0.2 < p_{\rm T} < 0.3$ Gev/c in the central rapidity bins for both space-time η and momentum y rapidities[2]. The times of the maximal emission extracted from the fits to interferometry radii are in good agreement with the presented HKM emission picture. As one can notice, the kaon radiation has two maxima: the first one at the proper time $\tau = 10$ fm/c and the second, broader and less pronounced, is at $\tau \approx 14$–15 fm/c. The origination of this second local maximum must be connected with decays of strange $K^*(892)$ resonance into $K\pi$ pairs containing additional $K^{\pm}(493.7)$ particles. Then, how the single obtained fit parameter $\tau_K \approx 12$ fm/c should be interpreted? Apparently, it can be understood as some effective (or mean) maximal emission time for kaons, corresponding to the actual two emission time maxima.

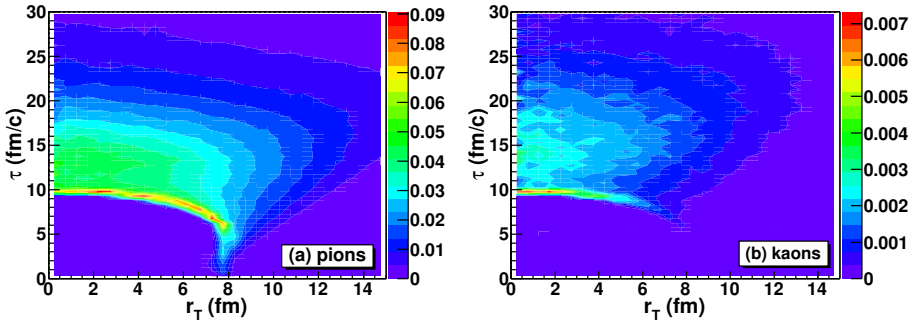

Fig. 5. The momentum angle averaged emission functions per units of space-time and momentum rapidities $g(\tau, r_{\rm T}, p_{\rm T})$ [fm^{-3}] (see the body text) for pions (a) and kaons (b) obtained from the HKM simulations of Pb+Pb collisions at the LHC $\sqrt{s_{NN}} = 2.76$ GeV, $0.2 < p_{\rm T} < 0.3$ GeV/c, $|y| < 0.5$, $c = 0$–5%.

This "mean" time is larger than the time of pion maximal emission, and the inequality between two values is much bigger in the case when hadron re-scatterings are switched on in the model ("full" mode). Such peculiarity can be explained by the consideration that in the regime when only resonance decays are implemented, the additional kaon emission source leads only to deviation of the CF shape from the Gaussian one, since fast K^* free streaming with subsequent decays into $K^{\pm}$ does not remind the hydrodynamic expansion of fluid elements, forming the source of primary kaons. In contrast, the re-scattering stage supposes that K^*s are involved in some kind of collective motion, thus affecting the longitudinal radius connected with the maximal emission time.

[2] Such a form of the emission function, in *out* and *side* $r_{\rm T}$ components, was used in [19–21] when deriving the analytical approximation for the correlation function.

As a result of performed fitting for the full HKM R_{L} points and the HKM momentum spectra, we arrive at different T and α parameter values for pions and kaons. It means that re-scatterings and resonance decays also lead to the m_{T}-scaling destruction along with already mentioned strong transverse flow. The influence of the re-scattering on violation of m_{T}-scaling was also noted in [24].

Now, let us return again to the HKM *long* radii behavior fitting. Previously considered points were extracted from the Gaussian fits to HKM correlation functions in a reduced q-range, q = 0–0.04 GeV/c. However, in the experimental analysis, one typically utilizes a broader interval, *e.g.* q = 0–0.2 GeV/c [25]. Applying (8) for fitting the HKM radii obtained using such extended range for q, one still gets a good description for pions (Fig. 6, gray/red line) with parameters constrained by combined spectra fit (T_π = 141 MeV, α_π = 1.82, τ_π = 10.34 ± 0.06 fm/c), but for kaons (T_K = 141 MeV, α_K = 1.5, and τ_K = 11.09 ± 0.02 fm/c), the description is unsatisfactory (see Fig. 6, solid black/blue line). In order to get an adequate fit for the kaon femtoscopy radii related to a wide q-region, one should remove restrictions on the α_K parameter. In Fig. 6, such a fit is demonstrated with the temperature $T = 144 \pm 3$ MeV still constrained, but with free α_K and τ_K (dashed black/blue line). The extracted maximal emission time $\tau_K = 12.65 \pm 1.58$ fm/c at T = 146 MeV and $\alpha = 0.02$ is in good agreement with the previous results for narrow-q radii and the particle emission structure represented by Fig. 5.

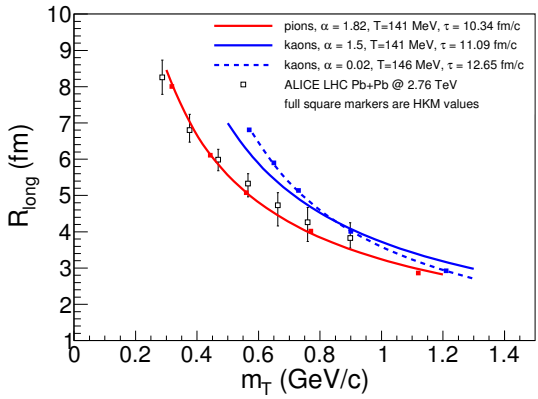

Fig. 6. The same as in Fig. 4, but the radii are extracted from the fits to full HKM correlation functions in a wide q range, q = 0–0.2 GeV/c. As one can see, the significant deviation of the CF shape from the Gaussian one leads to a distorted radii m_{T} behavior. At fitting, it can be compensated by decreasing α_K as compared to that obtained from the spectra fit. Experimental data [25] for pions are demonstrated for comparison.

As a conclusion, the longitudinal femtoscopy scales corresponding to the peak of the non-Gaussian correlation function can be well-described by the T and α parameters extracted from the combined pion and kaon spectra fit, giving a reliable estimate for the times of maximal particle emission. Still good estimates can be reached fitting the CF in a wide q range, however, the α_K parameter for kaons should be left unconstrained. As for the very small resulting α_K in this case, it can indicate that due to strong influence of the re-scattering processes at the afterburner stage of the collision, the interferometry radius m_{T} behavior cannot be described in a pure hydrodynamic approach. The deviation of the correlation function shape from the Gaussian one becomes more pronounced due to re-scatterings. Thus, the re-scattering stage plays a quite important role in m_{T} scaling violation.

In addition, we present the results for the source radii r_0 dependence on m_{T} for different meson and baryon particle pairs (see Fig. 7). These radii were extracted from the Gaussian fits to the angle-averaged HKM source functions $S(r) = 1/(4\pi)\int_0^{2\pi}\int_0^{\pi} S(r,\theta,\phi)\sin\theta \mathrm{d}\theta\,\mathrm{d}\phi$. The points in the figure present HKM points, and the lines show the fits (8) to these points. The parameter T at the fitting was constrained in accordance with the combined pion–kaon spectra fit result $T = 144 \pm 3$ MeV, while α and τ were left to vary freely. With the parameters $T = 141$ MeV for all the particle pairs, $\tau_{\pi\pi} = 11.47 \pm 0.03$ fm/c, $\tau_{KK} = 11.26 \pm 0.04$ fm/c, $\tau_{pp} = 11.30 \pm 0.13$ fm/c, $\tau_{p\Lambda} = 12.44 \pm 0.29$ fm/c, the fits describe the HKM results unexpectedly good. The parameter α for all the pairs is about 10^4 and more, *i.e.* actually $\alpha \to \infty$. This simply means that there are no transverse flows in the pair

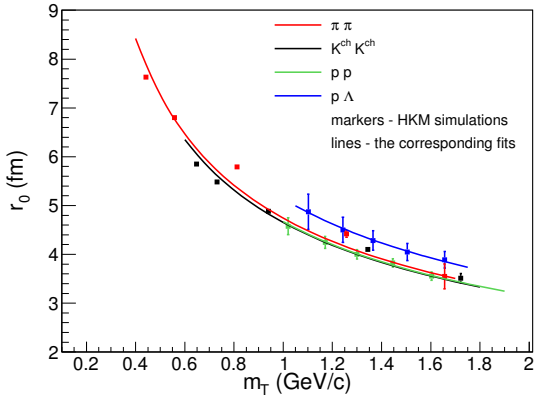

Fig. 7. The m_{T} dependencies of $\pi\pi$, $K^{\mathrm{ch}}K^{\mathrm{ch}}$, pp and $p\Lambda$ source radii r_0 extracted from corresponding angle-averaged source functions calculated in HKM for $\sqrt{s_{NN}} = 2.76$ GeV Pb+Pb collisions at the LHC, $c = 0$–5%, $|\eta| < 0.8$. Transverse momentum ranges are $0.14 < p_{\mathrm{T}} < 1.5$ GeV/c for pions and kaons, $0.7 < p_{\mathrm{T}} < 4.0$ GeV/c for protons and $0.7 < p_{\mathrm{T}} < 5.0$ GeV/c for Lambdas.

rest frame. The transverse velocity saddle point for fluid elements in rest is naturally zero. To our surprise, we see that for demonstrated radii, the m_{T}-scaling takes place.

3. Strange K^* resonance identification in iHKM

The clarification of the re-scattering stage role in the kaon emission picture is closely connected with the problem of $K(892)^*$ resonance experimental identification. Being itself the source of secondary kaons, the K^* can also serve as a probe for properties of the system, formed in heavy-ion collision at the late stages of its evolution.

In current section, we present the results of simulations in the integrated hydrokinetic model (iHKM) [26] concerning the $K(892)^*$ yields in Pb+Pb collisions at the LHC energy $\sqrt{s_{NN}} = 2.76$ TeV for the case of 8 centrality classes: $c = 0$–5%, $c = 5$–10%, $c = 10$–20%, $c = 20$–30%, $c = 30$–40%, $c = 40$–50%, $c = 50$–60%, and $c = 60$–70%. The iHKM model is an improved version of HKM, which includes, in addition to the latter, an energy-momentum transport model of the prethermal stage of the matter evolution in the collision and the viscous (not ideal as in HKM) hydrodynamics. The results below are obtained in the full publication being prepared [27].

Experimental identification of $K(892)^{*0}$ resonances is performed through the track forks of their decays into $K^+\pi^-$ pairs. Such restoration is complicated by several factors. First, because of comparably (with long-lived resonances) short $K(892)^*$'s lifetime (about 4 fm/c), the intensive re-scattering processes occurring at the "afterburner" stage of the matter evolution results in the two opposing effects:

(a) the reduction of the $K\pi$ pairs number identified as K^* due to momemtum diffusion of kaons and pions in the daughter pair, and

(b) the enhancement of K^* yield caused by pseudo-elastic interactions between hadrons, producing extra resonances.

Also the kaon–pion correlations of various origins, *e.g.* event-by-event elliptic flow and residual ones, are subject to misinterpretation and may be taken for the K–π bound state. The experimental misidentification issue also plays some role here. And at last, the imperfection of the invariant mass criterion, applied to the relevant $K\pi$ pairs selection may result in rejection of the pairs of interest or accept of the wrong pairs.

The joint impact of the first two competing effects on the K^* identification effectiveness can be studied within iHKM framework. For this purpose, one calculates the two K^* numbers: the number of actual K^{*0} particles, generated at the hadronization hypersurface and coming from the resonance

decays, and the number of $K^+\pi^-$ pairs, identified as coming from K^{*0} decay after the UrQMD cascade stage[3]. The rapidity and transverse momentum cuts for $K^+\pi^-$ pairs are chosen to be $|y| < 0.5$ and $0.2 < k_{\rm T} < 10$ GeV/c. We use the following criterion for the pair $K^+\pi^-$ relevance to K^{*0} decay: all the spatial coordinates of particle last collision points have to differ by less than 0.01 fm, $|x_i^K - x_i^\pi| < 0.01$ fm, while the pair invariant mass should differ from the invariant mass of $K(892)^{*0}$, which is $M_{K^*} = 895.94$ MeV, by less than 100 MeV.

The dependence of the fraction of "identified" K^*s obtained in iHKM on the collision centrality is demonstrated in Fig. 8 for Pb+Pb processes at the LHC energy $\sqrt{s_{NN}} = 2.76$ TeV. As one can see, this fraction increases from 0.78 for 5% most central collisions to 0.92 for the peripheral collisions with $c = 60$–70%. Actually, this is an expected behavior — in the central collisions rather extensive, hot and dense long-living system is formed, transforming subsequently into strongly re-scattering particles, that leads eventually to the problems with K^* identification. Such situation does not take place in the periphery collisions, where most of the nucleons in colliding nuclei pass near each other without intensive interaction, and effective interaction volume is relatively small.

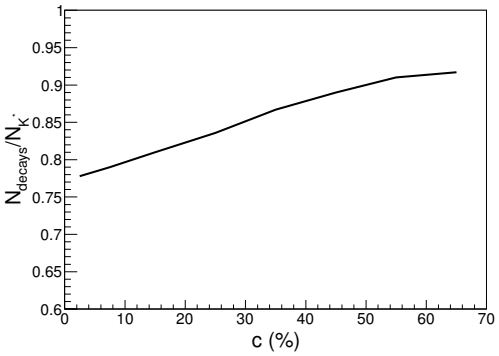

Fig. 8. The fraction of $K^+\pi^-$ pairs coming from $K(892)^*$ decay, which can be identified as K^* daughters in iHKM simulations after the particle re-scattering stage modeled within UrQMD hadron cascade. The simulations correspond to LHC Pb+Pb collisions at $\sqrt{s_{NN}} = 2.76$ TeV with different centralities.

The reason for the fraction of identifiable K^* not to reach unity even for essentially non-central collisions may lie in the imperfection of invariant mass criterion. Integrating the Breit–Wigner invariant mass distribution for $K(892)^{*0}$ in the range of $(M_{K^*} - 100\,\text{MeV}, M_{K^*} + 100\,\text{MeV})$, one will

[3] Usually in the experiment, the $\bar{K}^{*0}$ and $K^{*\pm}$ yields are analyzed as well, however our simulations show that the identification efficiency for these resonances is very close to the results for K^{*0}, so in what follows, we will mention only K^{*0}s, implying that the same concerns also $\bar{K}^{*0}$ and $K^{*\pm}$ resonances.

obtain the result close to 0.85. It means that in theory, only 85% of K^*s are restorable using the described criterion. A possible explanation of a larger value 0.92, obtained in iHKM, can be related to misidentification of $K\pi$ pairs, coming from other resonance decays with close invariant mass values and sufficiently large widths, as coming from $K(892)^{*0}$ decays.

The analogous model simulations for the long-living resonances, such as $\phi(1020)$ with lifetime about 50 fm/c which decays into K^+K^- and $K^0_{\rm L}K^0_{\rm S}$ pairs, demonstrate a rather good observability of this particles for all the considered centrality classes. The fraction of identified $\phi(1020)$ is even about 10% larger than unity, that can be the manifestation of KK correlations. Such a result indicate that lifetime of $\phi(1020)$ is much larger than the duration of the afterburner stage, so the re-scatterings do not reduce the yield of these resonances, rather opposite effect takes place: the recombination due to the KK interaction at active phase of the post-hydrodynamic stage is additional source of $\phi(1020)$.

The particle number ratios, such as K^*/K^+ ratio, can be the source of information about the dynamics of particle production in the heavy-ion collisions. Here, we demonstrate the K^*/K^+ number ratios calculated in the iHKM model for the LHC and RHIC energies. The calculations are performed at the two different stages: on the hadronization hypersurface (which is isotherm $T = 165$ MeV in our simulations), and in the end of hadron cascade stage. The primary K^*/K ratio values for all the considered centralities are about 0.5. The final-stage results are presented in Tables I and II and Fig. 9 for the Au+Au collisions at top RHIC energy and for Pb+Pb collisions at the LHC energy $\sqrt{s_{NN}} = 2.76$ TeV. The calculation results for RHIC are compared with the corresponding experimental data [28]. Here, kaon pseudorapidity cut is applied, $|\eta| < 0.8$, and selected kaon transverse momentum is limited to $0.2 < p_{\rm T} < 10$ GeV/c. As for the K^* resonances, they were again "reconstructed" from the decays into $K^+\pi^-$ pairs with $|y| < 0.5$ and $0.2 < k_{\rm T} < 10$ GeV/c. The iHKM calculations give the results that agree with the RHIC experimental analysis data within the errors, as it can be seen from the tables and figure. In both RHIC and LHC cases, the considered particle number ratio decreases approximately twice in the end of the collision as compared to the "primordial" result at the hypersurface of hadronization. The "afterburner" K^*/K ratio slightly increases when collision centrality is decreasing.

TABLE I

The comparison of K^*/K^+ ratio calculated in iHKM for the case of RHIC Au+Au collisions at $\sqrt{s_{NN}} = 200$ GeV and the experimental data [28] for different centrality classes.

c	K^*/K STAR	K^*/K iHKM
0–10%	$0.23 \pm 0.01 \pm 0.05$	0.21
10–30%	$0.24 \pm 0.02 \pm 0.05$	0.21
30–50%	$0.26 \pm 0.02 \pm 0.06$	0.22
50–80%	$0.26 \pm 0.02 \pm 0.05$	0.23

TABLE II

The K^*/K^+ ratio as calculated in iHKM for the case of LHC Pb+Pb collisions at $\sqrt{s_{NN}} = 2.76$ TeV for the events from different centrality classes.

c	K^*/K iHKM
0–5%	0.19
5–10%	0.19
10–20%	0.20
20–30%	0.20
30–40%	0.21
40–50%	0.22
50–60%	0.23
60–70%	0.24

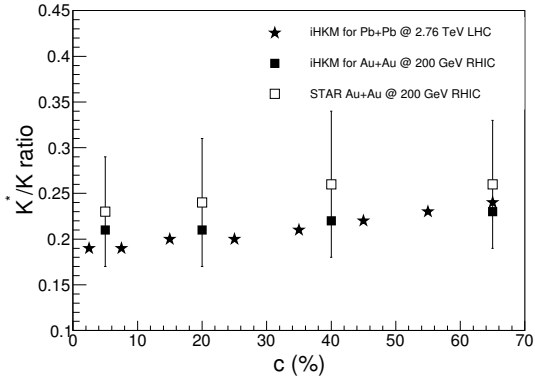

Fig. 9. The comparison of K^*/K^+ ratio calculated in iHKM for the case of RHIC Au+Au collisions at $\sqrt{s_{NN}} = 200$ GeV and the experimental data [28] for different centrality classes. The predictions for K^*/K^+ ratio in the LHC Pb+Pb collisions at $\sqrt{s_{NN}} = 2.76$ TeV for the events from different centrality classes are presented too.

4. Baryon–baryon correlations

This section is devoted to the theoretical description and predictions of baryon–(anti)baryon correlations induced by the strong and Coulomb final state interactions in such baryon pairs in relativistic heavy-ion collisions. The common approach to this issue is based on expressing the correlation function through the source function $S(\boldsymbol{r}^*)$ and the relative pair wave-function $\psi(\boldsymbol{r}^*, \boldsymbol{q}^*)$ using the so-called Koonin–Pratt equation [29–35]

$$C(\boldsymbol{q}^*) = \int \mathrm{d}^3 r^* S(\boldsymbol{r}^*) |\psi(\boldsymbol{r}^*, \boldsymbol{q}^*)|^2 \,. \tag{10}$$

At typical sizes of particle emission sources, formed in the high-energy collisions, if one studies the correlation between hadrons interacting solely strongly, the Lednicky–Lyuboshitz analytical model, utilizing the asymptotic expression for $\psi(\boldsymbol{r}^*, \boldsymbol{q}^*)$ at large distances, can be successfully used for analytical correlation function approximation [29]:

$$\Psi^S_{-\boldsymbol{k}^*}(\boldsymbol{r}^*) = e^{-i\boldsymbol{k}^*\cdot\boldsymbol{r}^*} + \frac{f^S(k^*)}{r^*} e^{ik^*\cdot r^*} \,, \tag{11}$$

$$\begin{aligned} C(k^*) = 1 + \sum_S \rho_S \Bigg[\frac{1}{2} \left| \frac{f^S(k^*)}{r_0} \right|^2 \left(1 - \frac{d_0^S}{2\sqrt{\pi} r_0} \right) \\ + \frac{2\,\mathrm{Re}\, f^S(k^*)}{\sqrt{\pi} r_0} F_1(2k^* r_0) - \frac{\mathrm{Im}\, f^S(k^*)}{r_0} F_2(2k^* r_0) \Bigg] \,, \end{aligned} \tag{12}$$

where $F_1(z) = \int_0^z \mathrm{d}x\, e^{x^2 - z^2}/z$ and $F_2(z) = (1 - e^{-z^2})/z$.

The particle strong interaction is characterized by the scattering amplitude $f^S(k^*)$, which in the effective range approximation is given by

$$f^S(k^*) = \left(\frac{1}{f_0^S} + \frac{1}{2} d_0^S k^{*2} - ik^* \right)^{-1} \,, \tag{13}$$

where f_0^S is the scattering length and d_0^S is the effective radius for a given total spin $S = 1$ or $S = 0$.

Fitting the experimental CF with (12) allows one to infer the unknown f_0^S and d_0^S parameters, defining the interaction within the pair. This procedure becomes improved if the source radius r_0, entering (12), is extracted from the Gaussian fit to the source function, calculated in realistic collision model. In the recent papers [36, 37], such an approach, based on the source functions calculated in HKM and supplemented with the method of effective accounting for residual correlations, was applied to the description of $p\Lambda$ and $\bar{p}\Lambda$ correlations in 10% most central Au+Au collisions at the top

RHIC energy [36] (see Figs. 10 and 11), and was used to make a prediction as for $p\Lambda$ CF in the 5% most central Pb+Pb collisions at the LHC energy $\sqrt{s_{NN}} = 2.76$ TeV [37] (see Figs. 12 and 13). The spin-averaged $p\Lambda$ scattering length value was extracted [36] from the fit to the RHIC experimental CF, measured by the STAR Collaboration [38].

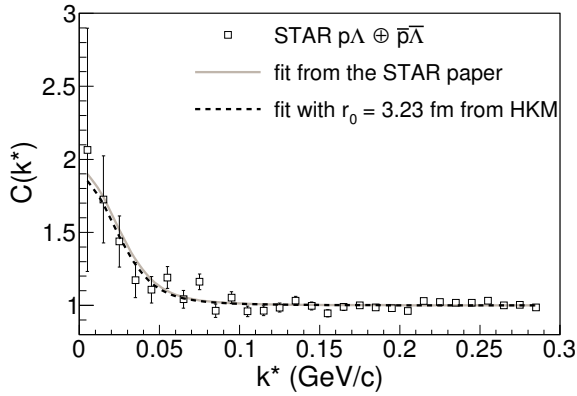

Fig. 10. The p–$\Lambda \oplus \bar{p}$–$\bar{\Lambda}$ correlation function measured by STAR (open markers), the corresponding fit according to (12) with parameters fixed as in the STAR paper [38] within the Lednický and Lyuboshitz analytical model [29] (gray solid line) and our fit within the same model with the source radius r_0 extracted from the HKM calculations (black dashed line).

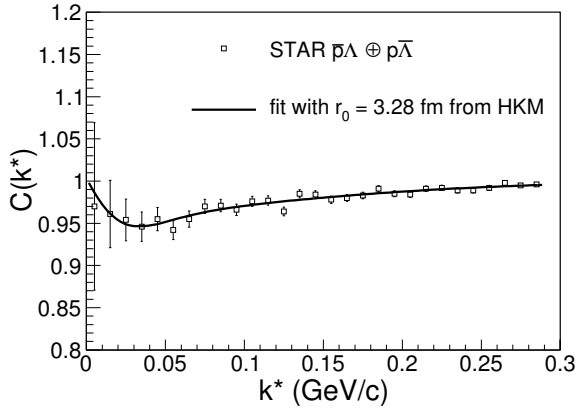

Fig. 11. The purity uncorrected $\bar{p}$–$\Lambda \oplus p$–$\bar{\Lambda}$ correlation function measured by STAR [39] (open markers) and our fit to it (black line), with the Gaussian parametrization (22) for the residual correlation term $C_{\rm res}(k^*)$. The source radius r_0 was fixed at a value extracted from the HKM calculations. The extracted fit parameters are $\mathrm{Re}\, f_0 = 0.14 \pm 0.66$ fm, $\mathrm{Im}\, f_0 = 1.53 \pm 1.31$ fm, $\beta = 0.034 \pm 0.005$ and $R = 0.48 \pm 0.05$ fm, with $\chi^2/\mathrm{n.d.f.} = 0.87$.

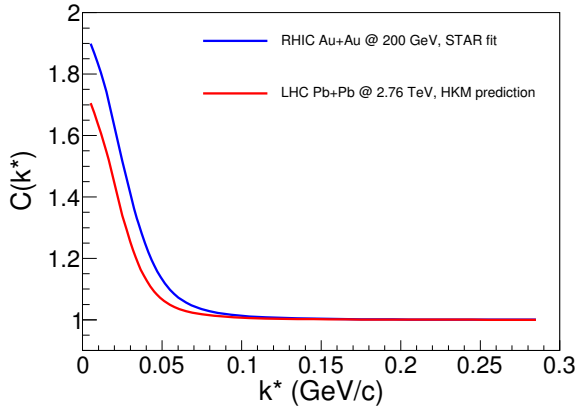

Fig. 12. The HKM prediction for purity corrected p–$\Lambda \oplus \bar{p}$–$\bar{\Lambda}$ correlation function in the LHC Pb+Pb collisions at $\sqrt{s_{NN}} = 2.76$ TeV, $c = 0$–5%, $|\eta| < 0.8$, with $0.7 < p_{\mathrm{T}} < 4$ GeV/c for protons and $0.7 < p_{\mathrm{T}} < 5$ GeV/c for Lambdas (gray/red line). The LHC source radius value calculated in HKM is $r_0 = 3.76$ fm. The Lednický–Lyuboshitz fit to the top RHIC energy correlation function, corresponding to the STAR experiment [38], with $r_0 = 3.23$ fm extracted from the HKM source function is presented for comparison (black/blue line).

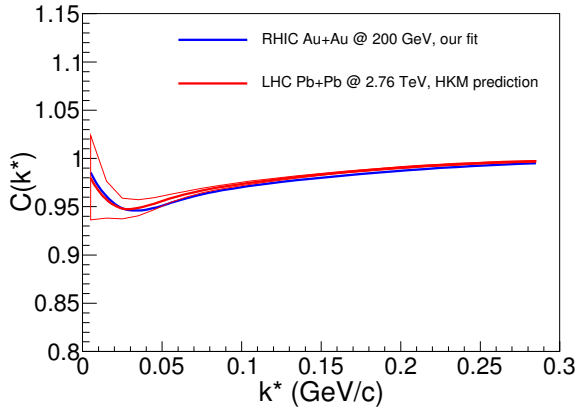

Fig. 13. The same as in Fig. 12 for purity uncorrected $\bar{p}$–$\Lambda \oplus p$–$\bar{\Lambda}$ correlation function. The HKM source radius for LHC is $r_0 = 3.76$ fm. The purity $\lambda(k^*)$ is the same as for the RHIC case [38]. The scattering length real and imaginary parts, $\mathrm{Re}\, f_0$ and $\mathrm{Im}\, f_0$, are taken from the fit to RHIC CF that corresponds to Fig. 6 from [36], where HKM source radius $r_0 = 3.28$ fm and the Gaussian parametrization (22) for the residual correlation contribution $C_{\mathrm{res}}(k^*)$ are utilized. For the LHC fit, the $C_{\mathrm{res}}(k^*)$ parameter β coincides with that for RHIC, while parameter R is scaled by the factor $r_0^{\mathrm{LHC}}/r_0^{\mathrm{RHIC}}$. The LHC fit is determined up to errors in parameters $\mathrm{Re}\, f_0$, $\mathrm{Im}\, f_0$, β and R, that is illustrated by the gray band around the LHC curve.

However, when we wish to apply the developed method to the description of the correlations in pairs, where the Coulomb interaction is also present, we should accordingly modify the theoretical formula for the correlation function. Following [40], we describe long-range Coulomb interaction with the amplitude

$$\psi_{-\boldsymbol{k}^*}(\boldsymbol{r}^*) = e^{i\delta_{\rm C}}\sqrt{A_{\rm C}(\eta)}\left[e^{-i\boldsymbol{k}^*\boldsymbol{r}^*}F(-i\eta,1,i\xi) + f_{\rm C}(k^*)\frac{\widetilde{G}(\rho,\eta)}{r^*}\right], \quad (14)$$

where $\xi = \boldsymbol{k}^*\boldsymbol{r}^* + k^*r^* \equiv \rho(1+\cos\theta^*)$, $\rho = k^*r^*$, $\eta = (k^*a)^{-1}$, $a = (\mu z_1 z_2 e^2)^{-1}$ is the two-particle Bohr radius including the sign of the interaction, $\delta_{\rm C} = \arg\Gamma(1+i\eta)$ is the Coulomb s-wave phase shift, $A_{\rm C}(\eta)$ is the Coulomb penetration factor,

$$F(\alpha,1,z) = 1 + \alpha z/1!^2 + \alpha(\alpha+1)z^2/2!^2 + \ldots \quad (15)$$

is the confluent hypergeometric function and $\widetilde{G} = \sqrt{A_{\rm C}}(G_0 + iF_0)$ is a combination of the regular (F_0) and singular (G_0) s-wave Coulomb functions

$$\widetilde{G}(\rho,\eta) = P(\rho,\eta) + 2\eta\rho\left[\ln|2\eta\rho| + 2C - 1 + \chi(\eta)\right]B(\rho,\eta)\,. \quad (16)$$

Here $C \doteq 0.5772$ is the Euler constant, the functions

$$\begin{aligned} B(\rho,\eta) &= \sum_{s=0}^{\infty} B_s\,, \qquad B_0 = 1\,, \qquad B_1 = \eta\rho\,, \qquad \ldots \\ P(\rho,\eta) &= \sum_{s=0}^{\infty} P_s\,, \qquad P_0 = 1\,, \qquad P_1 = 0\,, \qquad \ldots \end{aligned} \quad (17)$$

are defined by the following recurrence relations:

$$\begin{aligned} (n+1)(n+2)B_{n+1} &= 2\eta\rho B_n - \rho^2 B_{n-1}\,, \\ n(n+1)P_{n+1} &= 2\eta\rho P_n - \rho^2 P_{n-1} - (2n+1)2\eta\rho B_n\,, \end{aligned} \quad (18)$$

$B(\rho,\eta) \equiv F_0/(\rho\sqrt{A_{\rm C}}) \to \sin(\rho)/\rho$ and $P(\rho,\eta) \to \cos(\rho)$ in the limit $\eta\rho \equiv r^*/a \to 0$. The function

$$\chi(\eta) = h(\eta) + iA_{\rm C}(\eta)/(2\eta)\,, \quad (19)$$

where the function $h(\eta)$ is expressed through the digamma function $\psi(z) = \Gamma'(z)/\Gamma(z)$ as follows

$$h(\eta) = \left[\psi(i\eta) + \psi(-i\eta) - \ln\left(\eta^2\right)\right]/2\,. \quad (20)$$

Composing the full relative wave function as a superposition of the Coulomb (14) and strong interaction (11) amplitudes and substituting the result into (10), where the source function is a Gaussian fit $S_{\rm fit}(r^*) = (2\sqrt{\pi}r_0)^{-3}e^{-\frac{r^{*2}}{4r_0^2}}$ to the one-dimensional HKM source function $S(r^*) = 1/(4\pi)\int_0^{2\pi}\int_0^{\pi} S(r^*,\theta,\phi)\sin\theta \mathrm{d}\theta\,\mathrm{d}\phi$, one gets the analytical equation for the correlation function. This equation is rather complicated, so we do not list it here, limiting our presentation by the results of numerical calculations based on it.

In what follows, we consider some of results obtained in preparing full publication [41], the case of $p\Xi^-$ correlation function in the 5% most central Pb+Pb LHC collisions at the energy $\sqrt{s_{NN}} = 2.76$ TeV. To account for the residual correlation effect, we follow the procedure developed in [36, 37]. Having a correlation function not corrected for purity, we fit it with the formula

$$C_{\rm uncorr}(k^*) = 1 + \lambda(k^*)(C(k^*) - 1) + \alpha(k^*)(C_{\rm res}(k^*) - 1)\,, \qquad (21)$$

where $\lambda(k^*)$ is the pair purity or the fraction of correctly identified pairs consisting of primary particles, $C(k^*)$ is "true" correlation function obtained according to (10), $\alpha(k^*)$ is the fraction of secondary particles which are residually correlated, $\alpha(k^*) = \tilde{\alpha}(1 - \lambda(k^*))$ and $C_{\rm res}(k^*)$ is the residual correlation contribution. We take the latter in the Gaussian form [36, 37, 42]

$$C_{\rm res}(k^*) = 1 - \tilde{\beta}e^{-4k^{*2}R^2}\,, \qquad (22)$$

where $\tilde{\beta} = A > 0$ is the annihilation (wide) dip amplitude and $R \ll r_0$ is the dip inverse width. One can notice that $\tilde{\alpha}$ and $\tilde{\beta}$ enter (21) only as a product $\tilde{\alpha}\tilde{\beta}$, so that it can be treated at fitting as a single parameter β.

In Figs. 14–16, one can see our predictions for the $p\Xi^-$ and $p\Xi^+$ correlation function at the LHC. In the calculations, we use the source radius extracted from iHKM source functions for $p\Xi$ pairs, $r_0 = 3.1$ fm. Strong interaction scattering lengths and effective radii are assumed to be the same as for $p\Lambda$ pairs in [43] ($f_0^s = 2.88$ fm, $f_0^t = 1.66$ fm, $d_0^s = 2.92$ fm, $d_0^t = 3.78$ fm) and as obtained for $\bar{p}\Lambda$ in [36] (Re $f_0 = 0.14 \pm 0.66$ fm and Im $f_0 = 1.53 \pm 1.31$ fm, $d_0 = 0$). The parameters R and β describing residual correlations are taken from [37], $\beta = 0.034 \pm 0.005$ and $R_{\rm LHC} = 0.55 \pm 0.06$ fm. In the first figure, we present "true" CF, corresponding to the case of pair purity $\lambda = 1$ for two cases: application of the described FSI formalism at all the distances r between p and Ξ^- in the pair rest frame, and both Coulomb and strong interactions switched off at small distances $r < 1$ fm. The second figure shows the correlation functions $p\Xi^-$ with λ different from unity. Here, similarly

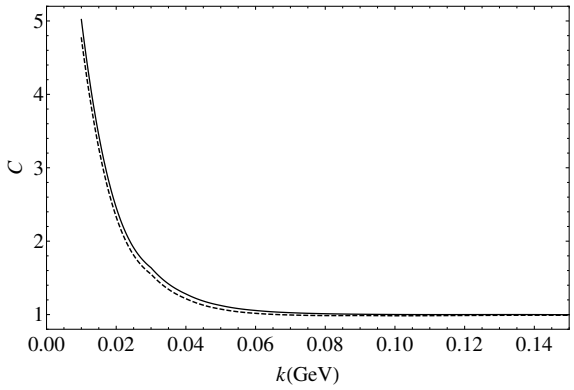

Fig. 14. The pure (purity $\lambda = 1$) baryon–baryon correlation function between primary proton and cascade, $p\Xi^-$ obtained in iHKM simulations. The Gaussian radius in the source function distribution in iHKM is 3.1 fm. The scattering lengths for strong interactions are supposed to be the same as in p–Λ systems. The solid line is related to assuming the Coulomb plus strong FSI exist at all distances r between the two baryons in the rest system of the pair. The dashed line corresponds to switching off all interactions at $r < 1$ fm. Therefore, the realistic results, accounting for the baryon kernel in short-range interaction and electromagnetic form-factors of baryons is supposed to be between these two curves.

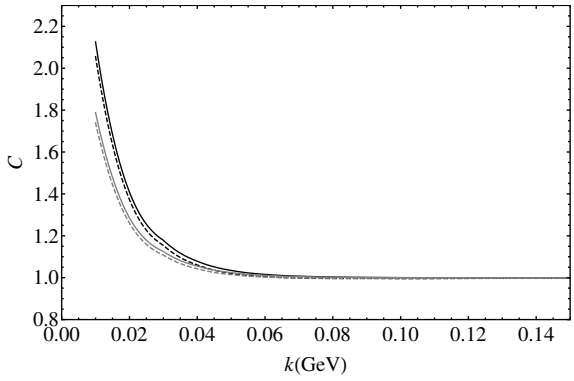

Fig. 15. The prediction for observed baryon–baryon correlation function proton and cascade, $p\Xi^-$ obtained in iHKM simulations. The purity that is result of long-lived resonance decays is found in iHKM as $\lambda_{\rm res} = 0.28$. The gray lines account in addition for the purity connected with particle misidentification and some other detector aspects. We put this additional factor as 0.7, so that the gray lines are corresponding to $\lambda = 0.7\,\lambda_{\rm res} = 0.196$. The other notations and parameters as in Fig. 14.

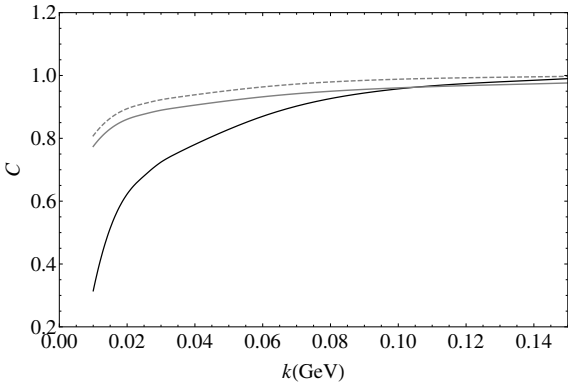

Fig. 16. The baryon–antibaryon correlation function for primary proton and anti-cascade, $p\Xi^+$, obtained in iHKM simulations. The Gaussian radius in the source function distribution in iHKM is 3.1 fm. The scattering lengths for strong interactions are supposed to be the same as for $\bar{\Lambda}$ extracted from STAR data in Ref. [36]. The black solid line is related to purity $\lambda = 1$ in primary baryon–antibaryon system. The gray dashed line correspond to the purity that is result of long-lived resonance decays as it is found in iHKM, $\lambda_{\rm res} = 0.28$. Solid gray line corresponds to account for the residual correlations among primary parents of p or/and Ξ^+. The parameters of such a correction are taken from top RHIC energies [36] and adjusted for LHC space scale by using iHKM similarly to the way it was done for $p\Lambda$ in [37] .

to [37], we suppose purity to be close to the fraction of primary proton-cascade pairs in iHKM simulations, $\lambda = 0.28$ (see Table III), perhaps with some deviations from this value caused by different experimental issues. We

TABLE III

The fractions of $p\Xi^-$ pairs, primary and coming from different decays calculated in iHKM.

Pairs	Fractions [%]
$p_{\rm prim}$–$\bar{\Xi}^-_{\rm prim}$	28
p_{Λ}–$\bar{\Xi}^-_{\rm prim}$	12
p_{Σ^+}–$\bar{\Xi}^-_{\rm prim}$	2
$p_{\rm prim}$–$\bar{\Xi}^-_{\Xi(1530)}$	38
p_{Λ}–$\bar{\Xi}^-_{\Xi(1530)}$	16
p_{Σ^+}–$\bar{\Xi}^-_{\Xi(1530)}$	3
$p_{\rm prim}$–$\bar{\Xi}^-_{\Omega^-}$	< 0.7
p_{Λ}–$\bar{\Xi}^-_{\Omega^-}$	< 0.3
p_{Σ^+}–$\bar{\Xi}^-_{\Omega^-}$	< 0.1

try to effectively account for the latter using the scaling factor 0.7 for the gray curves in Fig. 15. In Fig. 16, the result for baryon–antibaryon case (*i.e.* for $p\Xi^+$ pairs) is demonstrated. The black solid line corresponds to pure CF, $\lambda = 1$, while dashed gray line is related to $\lambda = 0.28$. The solid gray line shows the model CF where the residual correlations effect was taken into account in the way described above.

5. Summary

We have overviewed the recent results on the analysis of meson and baryon emission structure in relativistic heavy-ion collisions, obtained within the hydrokinetic and integrated hydrokinetic models. The detailed spatiotemporal picture of particle emission that is calculated in HKM for the cases of top RHIC and LHC energy collisions allows one to describe the behavior of a wide class of bulk observables and investigate the physical nature of observed effects, revealing the peculiar properties of the matter formed in the collision, and the process of its evolution.

Using simple analytical approximations, one can, based on the results of numerical calculations, determine various characteristics of the particle emission process, in particular, the time of maximal emission for particles of different species, effective temperature, collective flow parameters. Varying the model parameters allows one to investigate the role of different factors on the eventually obtained results. Thus, the violation of $m_{\rm T}$ scaling in the longitudinal interferometry radii dependence between pions and kaons can be explained by the influence of strong transverse flow and hadron re-scatterings at the late stages of the radiating system's evolution. The resonance decays, being the source of secondary particles production, also make a contribution to the final emission picture. In such a way, the K^* resonance decays produce the additional amount of kaons which are then subject of intensive re-scatterings at the afterburner stage, that significantly affects the observed behavior of interferometry radii and the extracted maximal emission time.

The dynamics of such re-scattering processes can be probed with the study of K^* observability, the possibility to restore these resonances through the products of their decays. The iHKM simulations show that in central collisions at the LHC, up to 25% of produced $K(892)^*$ cannot be identified due to dissipation of their decay daughters. This implies a quite strong effect of the re-scattering stage on the experimental measurement results, in particular on the femtoscopy scales.

The model simulations also help in FSI correlation analysis, allowing to calculate the emission source functions and facilitate the related fitting procedure. Another useful model application is finding the realistic pair purity values and investigating the contribution of the different factors on

it. Taking into account also the residual correlation effect, one can describe or predict the correlation functions of interest within different analytical models. In this paper, we presented such predictions as for $p\Xi$ correlation functions at the LHC energy.

The research was carried out within the scope of the EUREA: European Ultra Relativistic Energies Agreement (European Research Group: "Heavy ions at ultrarelativistic energies") and is supported by the National Academy of Sciences of Ukraine (Agreements MVC2-2016 and F7-2016). The work is partially supported by the Tomsk State University Competitiveness Improvement Program. Yu.S. is grateful to ExtreMe Matter Institute EMMI/GSI for support and visiting professor position.

REFERENCES

[1] S. Pratt, *Phys. Rev. D* **33**, 1314 (1986).
[2] A.N. Makhlin, Yu.M. Sinyukov, *Sov. J. Nucl. Phys.* **46**, 345 (1987); *Z. Phys. C* **39**, 69 (1988).
[3] Yu.M. Sinyukov, *Nucl. Phys. A* **498**, 151 (1989).
[4] Y. Hama, S.S. Padula, *Phys. Rev. D* **37**, 3237 (1988).
[5] G.I. Kopylov, M.I. Podgoretsky, *Sov. J. Nucl. Phys.* **15**, 219 (1972); **18**, 336 (1973); **19**, 215 (1974).
[6] Iu.A. Karpenko, Yu.M. Sinyukov, K. Werner, *Phys. Rev. C* **87**, 024914 (2013) [arXiv:1204.5351 [nucl-th]].
[7] Iu.A. Karpenko, Yu.M. Sinyukov, *Phys. Lett. B* **688**, 50 (2010).
[8] Iu.A. Karpenko, Yu.M. Sinyukov, *Phys. Rev. C* **81**, 054903 (2010).
[9] V.M. Shapoval, P. Braun-Munzinger, Iu.A. Karpenko, Yu.M. Sinyukov, *Nucl. Phys. A* **929**, 1 (2014).
[10] V.M. Shapoval, Yu.M. Sinyukov, Iu.A. Karpenko, *Phys. Rev. C* **88**, 064904 (2013).
[11] V.M. Shapoval, P. Braun-Munzinger, Iu.A. Karpenko, Yu.M. Sinyukov, *Phys. Lett. B* **725**, 139 (2013).
[12] Yu.M. Sinyukov, V.M. Shapoval, V.Yu. Naboka, *Nucl. Phys. A* **946**, 227 (2016).
[13] S.A. Bass *et al.*, *Prog. Part. Nucl. Phys.* **41**, 255 (1998); **41**, 225 (1998); M. Bleicher *et al.*, *J. Phys. G* **25**, 1859 (1999).
[14] Iu.A. Karpenko, Yu.M. Sinyukov, K. Werner, *Phys. Rev. C* **87**, 024914 (2013).
[15] W. Broniowski, M. Rybczyński, P. Bożek, *Comput. Phys. Commun.* **180**, 69 (2009) [arXiv:0710.5731 [nucl-th]].
[16] S.V. Akkelin, Y. Hama, Iu.A. Karpenko, Yu.M. Sinyukov, *Phys. Rev. C* **78**, 034906 (2008).

[17] Yu.M. Sinyukov, S.V. Akkelin, Y. Hama, Iu.A. Karpenko, *Acta Phys. Pol. B* **40**, 1025 (2009).
[18] F. Cooper, G. Frye, *Phys. Rev. D* **10**, 186 (1974).
[19] S.V. Akkelin, Yu.M. Sinyukov, *Phys. Lett. B* **356**, 525 (1995).
[20] S.V. Akkelin, Yu.M. Sinyukov, *Z. Phys. C* **72**, 501 (1996).
[21] Yu.M. Sinyukov, S.V. Akkelin, A.Yu. Tolstykh, *Nucl. Phys. A* **610**, 278 (1996).
[22] M. Herrmann, G.F. Bertsch, *Phys. Rev. C* **51**, 328 (1995).
[23] B. Abelev *et al.* [ALICE Collaboration], *Phys. Rev. C* **88**, 044910 (2013).
[24] A. Kisiel, M. Gałażyn, P. Bożek, *Phys. Rev. C* **90**, 064914 (2014).
[25] J. Adam *et al.* [ALICE Collaboration], *Phys. Rev. C* **93**, 024905 (2016) [arXiv:1507.06842 [nucl-ex]].
[26] V.Yu. Naboka, S.V. Akkelin, Iu.A. Karpenko, Yu.M. Sinyukov, *Phys. Rev. C* **91**, 014906 (2015); V.Yu. Naboka, Iu.A. Karpenko, Yu.M. Sinyukov, *Phys. Rev. C* **93**, 024902 (2016) [arXiv:1508.07204 [hep-ph]].
[27] V.M. Shapoval, P. Braun-Munzinger, Yu.M. Sinyukov, in preparation.
[28] STAR Collaboration, *Phys. Rev. C* **71**, 064902 (2005) [arXiv:nucl-ex/0412019].
[29] R. Lednický, V.L. Lyuboshitz, *Yad. Fiz.* **35**, 1316 (1981) [*Sov. J. Nucl. Phys.* **35**, 770 (1982)]; in: Proc. of the International Workshop on Particle Correlations and Interferometry in Nuclear Collisions (CORINNE 90), Nantes, France, 1990, Ed. D. Ardouin, World Scientific, Singapore 1990, pp. 42–54; R. Lednicky, *J. Phys. G: Nucl. Part. Phys.* **35**, 125109 (2008).
[30] E. Fermi, *Z. Phys.* **88**, 161 (1934); translated in: F.L. Wilson, *Am. J. Phys.* **36**, 1150 (1968).
[31] S.E. Koonin, *Phys. Lett. B* **70**, 43 (1977).
[32] M. Gyulassy, S.K. Kauffmann, L.W. Wilson, *Phys. Rev. C* **20**, 2267 (1979).
[33] R. Lednický, V.V. Lyuboshitz, V.L. Lyuboshitz, *Phys. Atom. Nucl.* **61**, 2050 (1998); R. Lednický, *J. Phys. G: Nucl. Part. Phys.* **35**, 125109 (2008).
[34] R. Lednický, *Phys. Part. Nucl.* **40**, 307 (2009).
[35] R. Lednický, *Phys. Part. Nucl. Lett.* **8**, 965 (2011).
[36] V.M. Shapoval, B. Erazmus, R. Lednický, Yu.M. Sinyukov, *Phys. Rev. C* **92**, 034910 (2015).
[37] V.M. Shapoval, Yu.M. Sinyukov, V.Yu. Naboka, *Phys. Rev. C* **92**, 044910 (2015).
[38] J. Adams *et al.* [STAR Collaboration], *Phys. Rev. C* **74**, 064906 (2006).
[39] G. Renault for the STAR Collaboration, *Acta Phys. Hung. A* **24**, 131 (2005).
[40] R. Lednicky, *Phys. Part. Nucl.* **40**, 307 (2009) [arXiv:nucl-th/0501065].
[41] Yu.M. Sinyukov *et al.*, in preparation.
[42] L. Adamczyk *et al.* [STAR Collaboration], *Phys. Rev. Lett.* **114**, 022301 (2015).
[43] F. Wang, S. Pratt, *Phys. Rev. Lett.* **83**, 3138 (1999).